

## Cracklike Surface Instabilities in Stressed Solids

W. H. Yang and D. J. Srolovitz

*Department of Material Science and Engineering, The University of Michigan, Ann Arbor, Michigan 48019-2136*  
(Received 25 March 1993)

The surface of an elastically stressed solid is shown to undergo an instability in which deep, cracklike grooves form by surface diffusion. These grooves sharpen and accelerate as they deepen. The resultant morphology is an excellent agreement with recent experimental observation in several disparate materials systems.

PACS numbers: 68.35.Bs, 61.72.Bb, 62.20.Mk

The temporal evolution of the morphology of stressed solids can be fundamentally different from that of unstressed solids. The equilibrium morphology of unstressed solids is usually determined by the principle of minimization of energy. Such variational principles are inapplicable when morphology is determined during growth. For example, in solidification, the Mullins-Sekerka instability can lead to complex, far-from-equilibrium dendritic morphologies or deep surface grooves (during directional solidification). Just as a temperature or concentration gradient can overcome the surface energy and destabilize a planar solidification front, a stress in a solid is capable of destabilizing otherwise flat surfaces. Asaro and Tiller [1], Grinfeld [2], Srolovitz [3], and others [4,5] have performed linear stability analyses which show that the competition between elastic strain energy and surface energy can lead to the growth of surface profile perturbations at large stress, small surface tension, and/or long wavelength. Experimental investigations of this strain energy driven instability corroborate several of the theoretical predictions. Torii and Balibar [6] performed a series of experiments on nonhydrostatically stressed  $^4\text{He}$  crystals and found that above a threshold stress, large grooves form on the surface of the crystal via surface diffusion. A similar observation was made by Berrehar *et al.* [7] who showed that a uniaxially stressed, epitaxial single crystal film of polymerized polydiacetylene on a monomer substrate forms regular grooves or quasiperiodic "cracks." Recent experiments [8] have shown that ion implanted, compressively stressed  $\text{SiO}_2$  is susceptible to forming this same type of cracklike surface morphology. The recent observations of this cracklike surface morphology in such a wide variety of materials indicate that this morphology is probably quite common and does not depend on the detailed properties of the host material.

While the linear stability analyses do adequately predict the conditions for the onset of instability, they are incapable of predicting the nature of the experimentally observed morphology—i.e., the deep groove morphology. The importance of properly accounting for the dominant nonlinearities in evolution equations is widely recognized, based upon studies in other pattern formation contexts. In the present Letter, we present the results of a numerical study of the full nonlinear stress-driven surface insta-

bility problem. We demonstrate that a nominally flat surface profile of an elastically stressed solid can rapidly evolve into a cusped surface, with smooth tops and deep cracklike grooves by surface diffusion. This morphology is in excellent agreement with those seen experimentally [6,7].

Our analysis proceeds as follow. Using continuum elastic theory, we derive a set of general equations for the stress state within a uniaxially stressed semi-infinite solid bounded by a surface of arbitrary shape. A boundary integral equation method is employed to solve these equations and determine the strain energy density field. The strain energy density along the surface and surface energy are employed to determine the chemical potential based upon the thermodynamics of elastically stressed solids [9,10]. We assume that the matter transport mechanism that controls the evolution of the surface shape is surface diffusion. Finally, the resultant surface evolution equation is solved using a Galerkin finite element method.

Consider a two-dimensional, semi-infinite solid with a traction-free surface lying along  $y=h(x)$  [the solid occupies  $y < h(x)$ ]. We assume that the surface profile is periodic with wavelength  $\lambda$  [ $h(x)=h(x+\lambda)$ ] such that the solid is subjected to a lateral bulk stress  $\sigma^\infty$ . The displacement field  $u_i$  along the surface is given by an integral equation of the form

$$u_i(\xi) = 2 \left[ u_i^\infty(\xi) - \int_S \bar{T}_{ij}(x, \xi) u_j(\xi) dS(x) \right], \quad (1)$$

where  $u^\infty$  is the displacement associated with the uniform bulk stress  $\sigma^\infty$  and  $\bar{T}_{ij}$  is the elastic Green's function that satisfies the periodic boundary conditions [11]. The strain energy may be obtained from the stresses, which are related to Eq. (1) through Hooke's law and the definition of strain.

The chemical potential  $\mu$  along the surface of a stressed solid can be described as  $\mu = \mu^* + \gamma\Omega\kappa + \Omega\omega$ , where  $\mu^*$  is the chemical potential of the flat surface bounding the solid with bulk stress  $\sigma^\infty$ ,  $\gamma$  is the surface free energy,  $\Omega$  is an atomic volume,  $\kappa$  is the surface curvature, and  $\omega$  is the strain energy density evaluated at the surface. A nonuniform chemical potential along the surface sets up surface diffusion fluxes proportional to the chemical potential gradient. The velocity of the surface

(normal to itself)  $v_n$  is proportional to the flux divergence [9]

$$v_n = \frac{D_s \Omega \delta}{kT} \frac{\partial^2 \mu}{\partial s^2}, \quad (2)$$

where  $D_s$  is the surface diffusivity,  $kT$  is the thermal energy,  $\delta$  is the number of atoms per unit area in the plane normal to the flux direction, and the derivatives are evaluated along the surface. Equation (2) may be rewritten in terms of the surface profile  $h(x, t)$  as

$$\frac{\partial h}{\partial t} = D \frac{\partial}{\partial x} \left[ (1 + h_x^2)^{-1/2} \frac{\partial}{\partial x} (\gamma \kappa + \omega) \right], \quad (3)$$

where  $D = D_s \delta \Omega^2 / kT$ .

The evolution of the surface profile is determined by a hybrid numerical procedure that combines a numerical solution of the boundary integral equation for the elasticity [Eq. (1)] with a Galerkin finite element technique for solving the nonlinear surface evolution equation [Eq. (3)]. Exactly the same surface profile discretization is employed in both the elastic and evolution analyses. Cubic  $B$ -splines [12] are employed to describe the boundary geometry and to serve as interpolation functions to preserve the continuity of the derivatives. The Galerkin finite element method is used for transforming the surface kinetics equation from a partial differential equation to an initial value problem. The weak formulation of the evolution equation [Eq. (3)] is solved using a fourth-order Runge-Kutta explicit time integration procedure.

We first compare the stress states predicted by the perturbative and boundary integral methods for a small amplitude sinusoidal surface profile  $h_0 = A \cos(2\pi x/\lambda)$ .

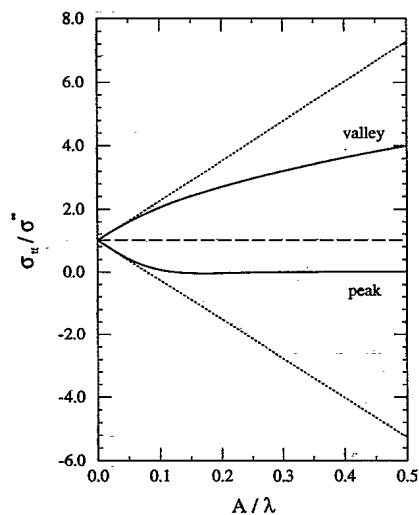


FIG. 1. The stress at the peak and valley of a sinusoidal surface profile as a function of the ratio of the amplitude to wavelength of that profile. The stresses are normalized by the far field stress. The solid lines represent the results of the present boundary integral equation method and the dotted lines represent the perturbation theory results.

When a tensile stress  $\sigma^\infty$  is applied parallel to the nominal surface, the maximum and minimum and tangential stresses occur at the valley and peak of the surface profile, respectively. The surface perturbation amplitude dependence of the tangential stress at the valley and peak positions along the surface are shown in Fig. 1. The lowest order perturbation solution [1-4] for the stresses at the valley and peak of the surface profile are  $\sigma^\infty [1 \pm 4\pi A/\lambda]$ . Although the perturbation analysis predicts that the peak stress is negative for  $A/\lambda > 1/4\pi$ , the boundary integral method shows that the  $\sigma_{tt}$  is always positive and approaches zero at large  $A/\lambda$ . The perturbative stress solution is only valid for small  $A/\lambda$  ( $< 0.1$ ). Gao [4] reached similar conclusions based upon a comparison of the perturbation solution with a (less accurate) finite element calculation of the stress concentration.

Figure 2 shows the temporal evolution of the surface profile of a uniaxially stressed solid (in the direction parallel to the nominal surface  $\sigma^\infty$ ) with  $A(t=0)/\lambda = 0.05$ . All stress and time variables are reported in scaled units:  $\Sigma = \sigma^\infty (\lambda/\gamma E)^{1/2}$  and  $\tau = \lambda^4/(D\gamma)$ . Figure 2 shows the temporal evolution of the surface under for  $\Sigma = 3$ . The surface profile evolves slowly from the initial cosine curve towards one with a pronounced groove at the minimum or valley in the initial surface profile. Once this groove forms, however, it grows rapidly. Two small bumps form immediately adjacent to the deep groove at long times.

Groove formation is attributable to the fact that the maximum stress and strain energy density occur at the position of the minimum in the initial surface profile. Since the chemical potential has a term which is linear in

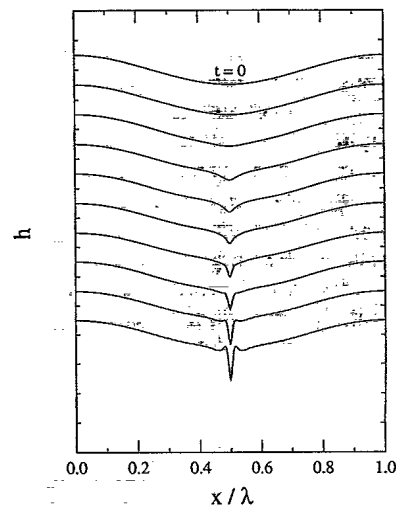


FIG. 2. The temporal evolution of the surface profile under the influence of a bulk stress  $\Sigma = 3$ . The initial surface profile is a sine wave with an amplitude to wavelength ratio of  $A_0/\lambda = 0.05$ . The different curves correspond to  $t = 0, 0.5 \times 10^{-3}\tau, 1 \times 10^{-3}\tau, 1.55 \times 10^{-3}\tau, 1.56 \times 10^{-3}\tau, 1.565 \times 10^{-3}\tau, 1.567 \times 10^{-3}\tau, 1.569 \times 10^{-3}\tau, \text{ and } 1.571 \times 10^{-3}\tau$ , from top to bottom.

the strain energy density, matter diffuses away from the minimum and, hence, the groove deepens. As the groove becomes deeper, the stress concentration at the groove root increases (as shown in Fig. 1) and the groove growth rate accelerates. The bumps that form adjacent to the deep groove are regions in which matter diffusing out of the groove accumulates. Their presence is a common feature of surface diffusion controlled surface morphology evolution (see, e.g., [9]).

If we approximate the groove as half of an ellipse, the stress field at the base of the groove may be described as  $\sigma_{tt}(x=\lambda/2) \approx \sigma^\infty(1+2a/b)$ , where  $a$  and  $b$  are the major and minor axes of the ellipse.  $a$  may be associated with the groove depth and  $b$  with the groove half-width. Returning to the sinusoidal perturbation of Fig. 1, we assign  $a=A$  and  $b=\lambda/2$ . This suggests that near the minimum in the sinusoidal perturbation  $\sigma_{tt} \approx 1+4(A/\lambda)$ . Figure 1 shows that  $\sigma_{tt}(x=\lambda/2)$  becomes linear for  $A/\lambda > 0.3$  and the slope is measured to be nearly 4, as predicted. This analysis confirms that for deep grooves, the stress and strain energy all increase at the groove tip with increasing groove depth and that the groove growth rate will accelerate with increasing groove depth.

The perturbation analysis yields  $A(t) = A(0)e^{\alpha t}$ , where the growth rate  $\alpha = D(2H\sigma^2 k^3 - \gamma k^4)$ ,  $k$  is the wave number of the perturbation and  $H = (1 - \nu^2)/E$  or  $1/E$  in plane strain or stress, respectively. Hence, the perturbation theory predicts that the surface is unstable for  $\sigma \geq \sigma_c = (\pi\gamma/H\lambda)^{1/2} \approx 1.88(\gamma E/\lambda)^{1/2}$ , where we have set  $\nu = \frac{1}{3}$ . The amplitude of the surface profile ( $h_{\max} - h_{\min}$ ) is shown as a function of time in Fig. 3 for several values of  $\sigma^\infty$ , where  $A(t=0)/\lambda = 0.05$ . The solid curves represent the results from the nonlinear, numerical analysis, while the individual data points represent the linear perturbation results [3]. The numerical results show that the surface perturbation decays for  $\Sigma=1$ , grows slowly for  $\Sigma=2$ , and quickly for  $\Sigma=2.5$  and 3, in agreement with the perturbation analysis. The linear analysis accurately predicts  $A(t)$  at low stresses/early times but greatly underestimates the groove growth rate at larger stresses. For  $\Sigma=1$  and 2, the surface profile remains smooth and grooveless for the times shown in Fig. 3, while for  $\Sigma=2.5$  and 3, the groove forms very early. The small discrepancy between the linear and nonlinear results for the growing  $\Sigma=2$  case is largely attributable to the increasing deviation of the surface profile from the sine curve as time increases.

The linear perturbation analysis fails dramatically (see Fig. 3) when a sharp groove forms. We can estimate the rate at which the groove deepens by surface diffusion using the elliptical groove approximation, described above. If we again approximate the groove as half of an ellipse with a constant radius of curvature  $\rho$  at its root, the growth rate of the major axis may be approximated as  $da/dt \approx [-\gamma + (\sigma^\infty)^2 Ha](D/\rho^3)$ , in the deep groove limit. When  $(\sigma^\infty)^2 aH/\gamma \gg 1$ , the groove growth rate is proportional to the groove size and  $a(t) \approx a(0)$

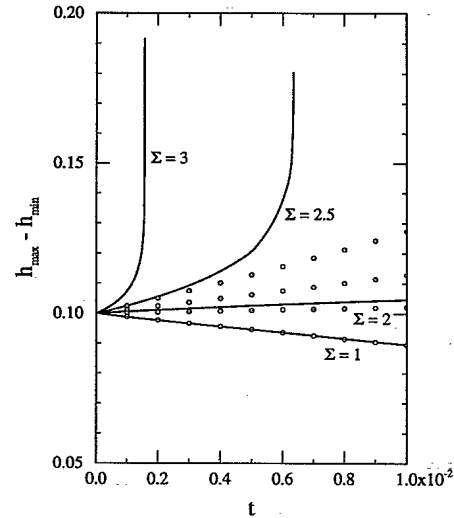


FIG. 3. The time dependence of the amplitude of the surface profile ( $h_{\max} - h_{\min}$ , in units of  $\lambda$ ) under the influence of several applied stresses  $\Sigma = 1.0, 2.0, 2.5$ , and  $3.0$ , from lowest to highest. The amplitude of the initial surface perturbation ratio  $A_0/\lambda = 0.05$ . The solid lines represent the results from the nonlinear surface evolution analysis. The data points (circles) correspond to the results of linear perturbation theory for the same wavelength and applied stresses.

$\times \exp[(\sigma^\infty)^2 HDt/\rho^2]$ . Figure 3 shows that after a short time, the groove growth rate rapidly accelerates (i.e., provided that the stress is sufficiently large for groove growth). This time dependence of the groove depth in Fig. 3 becomes faster than exponential. The failure of the semielliptical groove analysis is attributable to the failure of the assumption that the radius of curvature of the tip is independent of time.

In order to ensure that the rapid growth rate observed in Fig. 3 was not an artifact of the discretization of the surface in the numerical solution of Eq. (3), the numerical procedure was repeated with a significantly finer discretization. The finer discretization led to no qualitative changes in Fig. 3. However, the very rapid rise in  $h_{\max} - h_{\min} \approx a$  was shifted to slightly earlier times. The finer discretization also resulted in a very slightly sharper groove. A very fine time step  $\Delta t = 10^{-7} \tau$  was employed in the present calculations such that there are of order 100 points on the nearly vertical section of the  $\Sigma=3$  curve in Fig. 3.

The results presented show that the linear perturbation theory accurately predicts the onset of the stress driven surface morphology instability, in agreement with the recent experimental observations of epitaxial single crystal films of polymerized polydiacetylene [7] and  $^4\text{He}$  [6]. However, unlike the linear perturbation theory, the present nonlinear analysis clearly shows that the formation of the deep, cracklike groove morphology is the natural consequence of this stress-driven surface instability. The present analysis also suggests that the groove sharpens as it propagates and accelerates. This acceleration

cannot go on indefinitely and must be limited by the inherent discreteness of the atomic lattice. An atomically sharp groove is a crack.

The cracklike form of the stress-driven surface grooves suggests that there may be a connection between the stress-driven surface instability and the fracture process. In classical, brittle fracture mechanics (i.e., Griffith theory), a crack will grow if its length exceeds a critical size  $a > a^* \equiv 2E\gamma/\pi(\sigma^\infty)^2$ , where we have ignored dissipative mechanisms such as dislocation plasticity. In many cases, flaws present in the original material may be sufficiently large to propagate under the applied stress. Even when there are now flaws larger than  $a^*$  present, crack growth and delayed fracture may occur, especially at elevated temperatures. This delay must be associated with crack nucleation and/or subcritical crack growth. The mechanism by which cracks nucleate and grow subcritically is one of the most important deficiencies in our understanding of fracture.

The time required for a surface perturbation to grow into a supercritical crack depends on the surface diffusivity, applied stress, and the wavelength of the initial perturbation. In order to evaluate the significance of the proposed crack nucleation mechanism, we estimate the time required for a perturbation of the minimum unstable wavelength ( $\lambda_m = \gamma\pi/H\sigma^2$ ) to grow into a supercritical crack. Using the readily available physical data for copper and an applied stress  $\sigma^\infty = 10^{-3}E$ , we estimate the time required to grow a supercritical crack to be approximately 1 yr at 1000 K. We note, however, that appreciable surface roughness or local stress concentrators could drastically reduce this period. While this applied stress is sufficiently large to lead to plastic deformation in copper, in other materials, where dislocation motion is effectively inhibited (such as in materials with complex crystal structures), stresses of this magnitude may easily be achieved. Therefore, surface perturbations can grow into cracks under conditions typical of diffusional creep in materials where nondiffusional plastic deformation is inhibited.

There is a long history of analysis of crack nucleation and subcritical crack growth in stressed materials. Most of these earlier studies have focused on stress corrosion cracking [13,14] or the formation of creep cracks from voids [15,16]. In both cases, surface diffusion and/or chemical reactions have been shown to produce sharp "cracks" from voids or notches, when the stress is sufficiently large, or further blunting, otherwise. These conclusions are consistent with those presented here. However, the present results clearly demonstrate that crack nucleation can occur from a nominally flat surface without relying on the presence of macroscopic voids or notches to initiate fracture. Based upon the form of the chemical potential, Larché and Cahn [10] and Roitburd [16] suggested that necking of a sample in tension may be associated with a surface instability. The present paper demonstrates, through a nonlinear analysis, that this does

indeed occur and shows, for the first time, the manner in which this stress-driven surface instability leads to failure.

The present results demonstrate that the surfaces of elastic solids are unstable against surface diffusion controlled formation and subcritical growth of cracklike grooves. The very fast groove growth shown in Fig. 3 occurs when the groove is sufficiently sharp to behave like a crack and when its length exceeds  $a^*$ . In fact, inserting the parameters used in the present analysis into the expression for  $a^*$  shows that the groove growth rate diverges when its length is of order  $a^*$  (within a factor of 2). When  $\Sigma$  was decreased from 3 to 2.5 in Fig. 2, the size of the groove reached prior to unstable growth increases, in agreement with the expression for  $a^*$ . Once the crack exceeds the classical fracture criterion ( $a \geq a^*$ ), it will continue to propagate by bond breaking instead of by surface diffusion. This is the normal unstable crack growth of fracture mechanics. At this point, crack growth rates are limited by the speed of sound. Based upon their linear stability analysis over two decades ago, Asaro and Tiller [1] speculated that stress-driven surface instabilities may be related to the early stages of crack growth. The present results clearly demonstrate that this speculation was correct.

The authors gratefully acknowledge helpful discussions with L. B. Freund, M. A. Grinfeld, J. M. Rickman, C. F. Shih, and P. W. Voorhees. This research was supported by the Air Force Office of Scientific Research, Grant No. AFOSR-90-0141.

- 
- [1] R. J. Asaro and W. A. Tiller, *Metall. Trans.* **3**, 1789 (1972).
  - [2] M. A. Grinfeld, *Dokl. Akad. Nauk SSSR* **290**, 1358 (1986) [*Sov. Phys. Dokl.* **31**, 831 (1986)].
  - [3] D. J. Srolovitz, *Acta Metall.* **37**, 621 (1988).
  - [4] H. Gao, *Int. J. Solids Struct.* **28**, 703 (1991).
  - [5] B. J. Spencer, P. W. Voorhees, and S. H. Davis, *Phys. Rev. Lett.* **67**, 3696 (1991).
  - [6] R. H. Torii and S. Balibar, *J. Low Temp. Phys.* **89**, 391 (1992).
  - [7] J. Berrehar, C. Caroli, C. Lapersonne-Meyer, and M. Schott, *Phys. Rev. B* **46**, 3487 (1992).
  - [8] C. A. Volkert (private communication).
  - [9] W. W. Mullins, *J. Appl. Phys.* **28**, 333 (1957).
  - [10] F. C. Larché and J. W. Cahn, *Acta Metall.* **33**, 331 (1985).
  - [11] W. H. Yang and S. J. Srolovitz (to be published).
  - [12] C. de Boor, *A Practical Guide to Splines* (Springer-Verlag, New York, 1978).
  - [13] W. B. Hillig and R. J. Charles, in *High-Strength Materials* (Wiley, New York, 1965), p. 682.
  - [14] T. J. Chuang and E. R. Fuller, *J. Am. Ceram. Soc.* **75**, 540 (1992).
  - [15] J. R. Rice and T. J. Chuang, *J. Am. Ceram. Soc.* **64**, 46 (1981).
  - [16] A. L. Roitburd, *Fiz. Tverd. Tela* **23**, 1074 (1981) [*Sov. Phys. Solid State* **23**, 622 (1981)].